Geophysical Research Letters®

Correspondence to:

A. J. Wilson,
a.j.wilson1@leeds.ac.uk

Powering Earth's Ancient Dynamo With Silicon Precipitation

Alfred J. Wilson[1] [ID], Monica Pozzo[2,3] [ID], Dario Alfè[2,3,4] [ID], Andrew M. Walker[5] [ID], Sam Greenwood[1] [ID], Anne Pommier[6] [ID], and Christopher J. Davies[1] [ID]

[1]School of Earth and Environment, University of Leeds, Leeds, UK, [2]Department of Earth Sciences, University College London, London, UK, [3]London Centre for Nanotechnology, Thomas Young Centre, University College London, London, UK, [4]Dipartimento di Fisica "Ettore Pancini", Universita' di Napoli "Federico II", Monte S. Angelo, Napoli, Italy, [5]Department of Earth Sciences, University of Oxford, Oxford, UK, [6]Earth & Planets Laboratory, Carnegie Institution for Science, Washington, DC, USA

Abstract Earth's core has produced a global magnetic field for at least the last 3.5 Gyrs, presently sustained by inner core (IC) growth. Models of the core with high thermal conductivity suggest potentially insufficient power available for the geodynamo prior to IC formation ∼1 Ga. Precipitation of silicon from the liquid core might offer an alternative power source for the ancient magnetic field, although few estimates of the silicon partition coefficient exist for conditions of the early core. We present the first ab initio determination of the silicon partition coefficient at core-mantle boundary conditions and use these results to confirm a thermodynamic description of partitioning that is integrated into a model of coupled core-mantle thermal evolution. We show that models including precipitation of silicon can satisfy constraints of IC size, mantle convective heat flux, mantle temperature and a persistent ancient geodynamo, and favor an oxygen poor initial core composition.

Plain Language Summary The iron core at the center of the Earth presently has a molten outer shell and solid inner region which is growing as the Earth cools. This inner core (IC) growth provides power to the outer core (OC) because elements excluded from the IC are light and rise to the top of the OC. Today, this power drives the Earth's magnetic field but was not available before the IC began to freeze 1 billion years ago. Despite this, the rock record shows that the magnetic field has been extant for 4 billion years, raising the question of how it was powered before the IC formed. Here, we perform calculations of the constituent liquid iron alloys in the core to understand the conditions which allow silicon to be dissolved into the core. We find that for a low oxygen condition, silicon can be dissolved into the hot ancient core and then released as the Earth cools, leaving behind dense, iron rich liquids which sink providing an alternate source of convective power. We show that this process could have powered the magnetic field before the IC formed and might constrain the core composition.

1. Introduction

Earth's magnetic field is fundamental for the habitability of our planet, and yet the power to sustain it over Earth's history remains enigmatic. Palaeointensity data suggest the field has been maintained for at least the last 3.45 Gyrs (Tarduno et al., 2010) but the main power sources derive from growth of the solid inner core (IC) (Davies, 2015; Labrosse, 2015; Nimmo, 2015), which is thought to have formed only ∼1 Gyr ago. IC growth provides latent heat, however more influential is that light elements can be partitioned into the liquid (Braginsky, 1963) creating a chemical buoyancy source at the base of the outer core (OC). Oxygen is considered a likely candidate because it can help to explain the density contrast between the IC and OC (Alfè et al., 2002) although similar partitioning (PT) and convective influence can be explained by carbon (Li et al., 2019). Enrichment of the lowermost OC in light elements provides power for convection which is expected to be the major contributor to geodynamo power today (Buffett et al., 1996; Gubbins et al., 2004; Labrosse, 2015).

The thermal conductivity (k) of the core has been debated over recent years, with a wide range of published values from 20 W m^{-1} K^{-1} (Hsieh et al., 2020) to 130 W m^{-1} K^{-1} (de Koker et al., 2012; Gomi et al., 2013; Pozzo et al., 2012, 2013). Core thermal history based on the lower end of these estimates is well understood and implies that secular cooling is sufficient to power the geodynamo before IC formation (Nimmo, 2015). However, many recent studies (e.g., Davies & Greenwood, 2021; Pozzo et al., 2022; Zhang et al., 2022) favor $k = 70–110$ W m^{-1} K^{-1}. At such high k the core's thermal evolution is less well understood so we consider this

Writing – review & editing: Alfred J. Wilson, Monica Pozzo, Dario Alfè, Andrew M. Walker, Sam Greenwood, Anne Pommier, Christopher J. Davies

scenario in the remainder of this study. Nimmo (2015), Davies (2015) and Labrosse (2015) impose a core mantle boundary (CMB) heat flow and find that a higher k core requires faster cooling to sustain a geodynamo through secular cooling alone, implying super-solidus CMB in early times temperatures and a prolonged basal magma ocean (BMO). Nakagawa and Tackley (2013), Driscoll and Bercovici (2014) and O'Rourke et al. (2017) each use parameterisations of mantle convection to set CMB heat flow for core thermal history models and all find that sustaining the geodynamo in a high k core is challenging without additional power sources to supplement secular cooling. Davies and Greenwood (2021) find that powering the geodynamo by secular cooling alone is possible but requires a BMO to regulate CMB heat flow and is a rare case in parameter space. A robust power source for the ancient geodynamo therefore remains elusive.

In search of alternate power sources in the high k scenario, prior studies have investigated whether light elements incorporated into the core during a hot differentiation might become insoluble during cooling and precipitate. Convection is driven by dense, iron-rich residual liquids sinking following precipitation at the CMB. Lower initial core temperatures and slower cooling allowed by this power source imply a significantly older IC. MgO precipitation has been suggested (Badro et al., 2016, 2018; O'Rourke & Stevenson, 2016) although the dependence of magnesium solubility on the oxygen content of the core may reduce the overall power output (Du et al., 2017, 2019). Others have investigated the possibility of precipitating Si (Helffrich et al., 2020; Hirose et al., 2017) which is a more widely accepted component in the core (e.g., Fischer et al., 2015; Rubie et al., 2015; Takafuji et al., 2005) as well as simultaneous precipitation of multiple elements (Mittal et al., 2020). However, at present there is no consensus on the onset time or power derived from Si precipitation. This is due to uncertainties on the initial composition of the core (Badro et al., 2015; Fischer et al., 2017; Rubie et al., 2015), method of modeling the PT behavior, and lack of data at core conditions. Here we will address all three of these issues.

In this study we produce the first determinations of Si PT at CMB conditions using ab initio molecular dynamic simulations. We derive a thermodynamic model for Si PT using a data set which spans a wider range of physical and chemical conditions than was available to previous studies and confirm the extrapolation of this model to core conditions with our ab initio results. We use our thermodynamic model to describe Si precipitation in thermal history models of the cooling core. Previous studies that modeled the effect of Si precipitation from an Fe-Si-O system on the core's thermal evolution have evaluated the cooling rate needed to sustain the geodynamo without explicitly modeling the core evolution (Hirose et al., 2017; Zhang et al., 2022) and implemented a thermodynamic model of simultaneous precipitation of multiple light elements into a parameterized model of core thermal evolution (Mittal et al., 2020). We take a combined approach, using a thermal evolution model and focusing solely on Si precipitation, resolving complex compositional effects on Si solubility that were not investigated previously.

2. Methods

2.1. Ab Initio Calculations

We conduct density functional theory (Hohenberg & Kohn, 1964; Kohn & Sham, 1965) molecular dynamic simulations of silicate (close to pyrolitic composition) and iron-rich liquids to calculate the excess chemical potentials using methods from Pozzo et al. (2019) (see Supporting Information S1 for details). Chemical potentials (μ_i) can be described as the free energy change (∂F) of a system when the concentration of a species (x_i) is changed

$$\mu_i(v, T, x_j, \dots) = \left(\frac{\partial F}{\partial x_i}\right)_{V, T, x_j, \dots} \tag{1}$$

where v is partial molar volume and V is volume. Thermodynamic integration is used to calculate μ_i in two ways: by changing the number of solute atoms x_i, which directly provides $\partial F/\partial x_i$, and by using an external reference potential to calculate F at two different values of x_i, which again allows the evaluation of $\partial F/\partial x_i$. Each approach allows independent calculation of μ_i through Equation 1.

We find distribution coefficients (K_d) from our ab initio results of μ_i. When μ_i on either side of a reaction are equal, this component is in thermodynamic equilibrium and each concentration will be stable:

$$\mu_{SiO_2}^{silicate}\left(V, T, x_{SiO_2}^{silicate}, x_j^{silicate}, \dots\right) = \mu_{SiO_2}^{metal}\left(V, T, x_{SiO_2}^{metal}, x_j^{metal}, \dots\right). \tag{2}$$

Here μ_i is dependent on V, T and composition. Separating out the configurational portion of μ_i gives

$$2\left(k_B T \ln x_O^{silicate} + \tilde{\mu}_O^{silicate}\right) + k_B T \ln x_{Si}^{silicate} = 2\left(k_B T \ln x_O^{metal} + \tilde{\mu}_O^{metal}\right) + k_B T \ln x_{Si}^{metal} \qquad (3)$$

where $\tilde{\mu}_{SiO_2} = \tilde{\mu}_{Si} + 2\tilde{\mu}_O$ in the liquid, which when rearranged becomes equal to the distribution coefficient for a dissociation reaction

$$K_d^{dissociation} = \frac{x_{Si}^{metal} x_O^{metal\,2}}{x_{SiO_2}^{silicate}} = \exp\left(-\frac{\tilde{\mu}_{SiO_2}^{metal} - \tilde{\mu}_{SiO_2}^{silicate}}{k_B T}\right). \qquad (4)$$

Exchange and dissolution reactions are also possible, see Supporting Information S1 for analysis of each reaction. We focus on pressure, temperatures (124 GPa, 4500–5500 K) and compositions relevant to the CMB as these are the most crucial for the evolution of the core.

2.2. Thermodynamic Model

We use an interaction parameter model (Ma, 2001) commonly applied to high PT reactions (e.g., Badro et al., 2018; Fischer et al., 2015; Hirose et al., 2017; Liu et al., 2020) to describe the solubility of Si in iron-rich liquids and broaden the utility of our ab initio results. We consider dissolution, dissociation and exchange reactions (Equations S4, S3, S4 in Supporting Information S1), and fit each as a thermodynamic model (Equation S8 in Supporting Information S1) to experimental values of K_d. The interaction parameters of these models are able to capture the effects of C, O, Si, S and Mg content of the metal on Si solubility (chosen to represent likely light elements in the core and to account for common impurities in our experimental data set) unlike our ab initio results. Dissociation (Equation 4) is found to best explain the compositional effects of our data set and we consider this reaction for our thermodynamic model. Details of each reaction are provided in the Supporting Information S1.

The stable fraction of Si in the liquid metal to be evaluated for the dissociation reaction through

$$x_{Si}^{metal} = \exp\left(a + \frac{b}{T} + c\frac{P}{T} + \log x_{SiO_2}^{silicate} - 2\log x_O^{metal} - 2\ln\gamma_O - \ln\gamma_{Si}\right) \qquad (5)$$

where γ_x are constructed from interaction parameters (Equation S9 in Supporting Information S1) and account for the deviation from ideal PT due to composition. Interaction parameters are notionally universal and constant, but in reality, data are insufficient to fully resolve all possible parameters. This is because the existing data do not fully span P, T and composition space for the core. Varying starting compositions among studies also limits the interactions which can be resolved and affects model behavior because omission of one element can affect the predicted interactions between retained elements. Additionally, differing experimental techniques introduce various uncertainties which will be incorporated into fitted interaction parameters and the interaction parameter model is designed for, and suited to, solutes at lower concentration than some experimental studies investigate. It is therefore inevitable that the interaction parameters will vary based on these factors, as can be seen by comparing results from previous studies (Badro et al., 2018; Fischer et al., 2015; Liu et al., 2020; Zhang et al., 2022) as well as in this study. To mitigate these difficulties, we have gathered a larger data set than was available to previous studies (480 measurements from 33 studies) in order to better constrain Si PT behavior. Details of the thermodynamic model, reaction pathway, experimental data set and fitting can be found in the Supporting Information S1.

2.3. Thermal Evolution Model

Thermal evolution modeling follows Davies (2015) where, if small terms are ignored, the heat flow across the CMB (Q_{cmb}) is found through the balance of energies

$$Q_{cmb} = Q_s + Q_L + Q_{ppt}^{Si} + Q_g. \qquad (6)$$

Q_s is the secular heat stored in the core, Q_L is the latent heat release due to IC growth and Q_g is the gravitational power generated from the preferential PT of O into the lowermost liquid core upon freezing. Q_{ppt} is the gravitational energy from mixing the dense, iron-rich residual liquids produced by the precipitation process across the OC (O'Rourke & Stevenson, 2016) and is given by

$$Q_{ppt}^{Si} = \int_{V_c} \psi \rho \alpha_{ppt}^{Si} \left[C_{ppt}^{Si} \left(\frac{dT_{cmb}}{dt} \right) \right] dV_c \qquad (7)$$

where ρ is density, α_{ppt}^{Si} is expansivity, ψ is gravitational potential, $C_{ppt}^{Si} = \frac{dx_{Si}^{metal}}{dT_{cmb}}$ is the precipitation rate of Si, T_{cmb} is the CMB temperature, t is time and V_c is volume of the liquid core (parameter values are specified in the Supporting Information S1). We use our thermodynamic model to evaluate C_{ppt}^{Si} from T, P and x. x_{Si}^{metal} is reduced to the thermodynamically stable fraction, treating the excess as precipitate. Si precipitation is considered over SiO_2 to isolate its effect on thermal evolution and also to avoid the need to include a description of phase (e.g., SiO_2 or SiC) or source of reactant (e.g., mantle or core) both of which are highly uncertain. We assume Si to partition evenly between the solid and liquid core (Alfè et al., 2002) such that the growth of the IC has no direct effect on the Si concentration of the liquid core. The entropy budget of the core can be balanced (Gubbins et al., 2004) by

$$E_j + E_k = E_s + E_L + E_{ppt}^{Si} + E_g, \qquad (8)$$

again neglecting small terms. E_k is the entropy from thermal conduction and the other terms follow the same notation as their energy counterparts. E_j is the entropy due to ohmic dissipation, which is an output of the model and must be positive for dynamo action.

3. Results

Si distribution coefficients $\left(K_d^{dissociation} \right)$ are calculated from first principles for the first time at conditions of the early core using excess chemical potentials. We obtain $K_d^{dissociation} = 0.50_{+0.1}^{-0.09}$ at 5500 K and $0.029_{+0.028}^{-0.014}$ at 4500 K, both at 124 GPa. Because each P, T, x point requires several million hours of CPU time, we are restricted here to two points. The ab initio results of this study agree well with experiments, Figure 1 shows the experimental $K_d^{dissociation}$ from our data set where our result at 4500 K which lies within the scatter of experiments at similar temperatures. At 5500 K there are very few data, but if the scatter is similar then our result would also be consistent with Fischer et al. (2015) and Chidester et al. (2017). This data set shows a strong temperature dependence and a weaker pressure effect (Figure S1 in Supporting Information S1 shows the full distribution of the data set), especially above 50 GPa, commensurate with an entropy dominated, configurational change in the iron-rich liquid when incorporating light elements, in agreement with other high PT studies (e.g., Badro et al., 2018; Fischer et al., 2015).

The temperature dependence of Si solubility predicted by our thermodynamic model (Equation 5) at 5000 K is $\frac{dx_{Si}^{metal}}{dT} = 0.0014$ K^{-1}, which is within the uncertainty of our ab initio results (0.0016–0.00086 K^{-1}). Interaction parameters which define γ_i of the model are reported in Supporting Information S1. The dominant compositional effect is that O limits the solubility of Si (cf. Hirose et al., 2017; Zhang et al., 2022). Figure 2 explores the prediction of stable Si concentration and precipitation rate from our thermodynamic model with different x_O^{metal} conditions. For a 38.8 mol% SiO_2 silicate equilibrated with iron liquids at moderate O concentrations (between dashed and dotted lines, Figures 2, 0.4–1 wt.%) and temperatures between 3500 and 6000 K, we find precipitation rates of 2×10^{-3}–3×10^{-4} wt.% K^{-1}.

To test the robustness of our results we refit our model using the interaction parameters from Fischer et al. (2015) and Badro et al. (2018). The resulting precipitation rates fall within the red hatched area of Figure 2, meaning that the uncertainty of the amount of O in the core is more significant than the uncertainty of interaction parameters in our model.

One notable implication of our model is that the range of initial Si concentrations predicted by core formation models (blue shaded areas, Badro et al., 2015; Fischer et al., 2017; Rubie et al., 2015) will evolve to encompass the Si content of Fe-S/Si-O systems found to be consistent with IC density jumps of 0.8 and 1.0 g cm^{-1} but not 0.6 g cm^{-1} (orange points, Davies et al., 2015). More complex metal compositions do affect the solubility of Si in the liquid; however, we do not explore these in this study because temperature and O content have a far greater effect than the C, S, Mg or pressure effects we resolve.
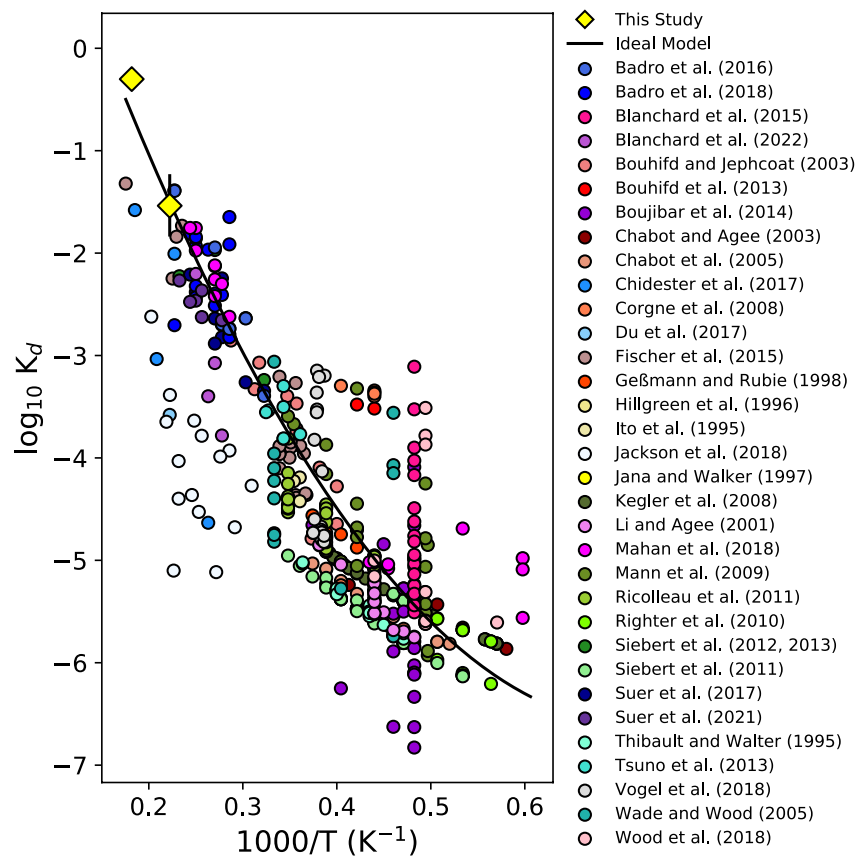
Figure 1. Comparison of $K_d^{dissociation}$ for Si into Fe-rich liquid calculated from our experimental data set using our thermodynamic model with ab initio results of this study (yellow diamonds). For simple comparison, our thermodynamic model is evaluated for $K_d^{dissociation}$ in an ideal condition, where all $\gamma_i = 0$ (black line, $x_O = 2$ mol.%, 124 GPa).

4. Discussion

4.1. Thermal Evolution of the Core

To investigate the effect of Si precipitation on the thermal evolution of the core we combine two classical models, one of the core (Davies & Greenwood, 2021; Greenwood et al., 2021) and one of the solid mantle (Driscoll & Bercovici, 2014). These parameterisations of the deep Earth are coupled at the CMB, where the mantle defines Q_{cmb} and the core defines T_{cmb}. A moderately high k scenario is considered, where $k = 70$ W m^{-1} K^{-1} everywhere in the core (Davies & Greenwood, 2021; Pozzo et al., 2022). Whilst this k is higher than some published values, it represents a low value amongst recent results (see Pozzo et al., 2022, for a detailed discussion).

We assume that the core is mixed thoroughly on timescales far shorter than the timestep of our simulation such that the liquid core has no compositional variation nor chemically stable layers as is standard for these types of models (Nimmo, 2015). Mantle composition is held constant for simplicity, reflecting the situation studied by Helffrich et al. (2020) where light precipitates rapidly rise into the mantle. We do not include other reactions with the mantle which would alter the Mg and O concentration of the core as this would involve additional description of reactions and fitting of γ^0 parameters, which is beyond the scope of this study. We note that such a consideration would not necessarily benefit our investigation of the effect of Si precipitation on the thermal history of the core, but would help constrain the composition of the core through time.

We consider two compositional scenarios to explore a range of possible initial conditions; one with a high initial O content (10 mol%) and one with a low initial oxygen content (2 mol%) in the liquid core, each in contact with a 38.8 mol.% SiO_2 mantle. Table S5 in Supporting Information S1 provides the details of each case. Each initial core composition is evolved under conditions of initially over- (A, A^P, C, C^P) and under-saturated (B, B^P, D, D^P)
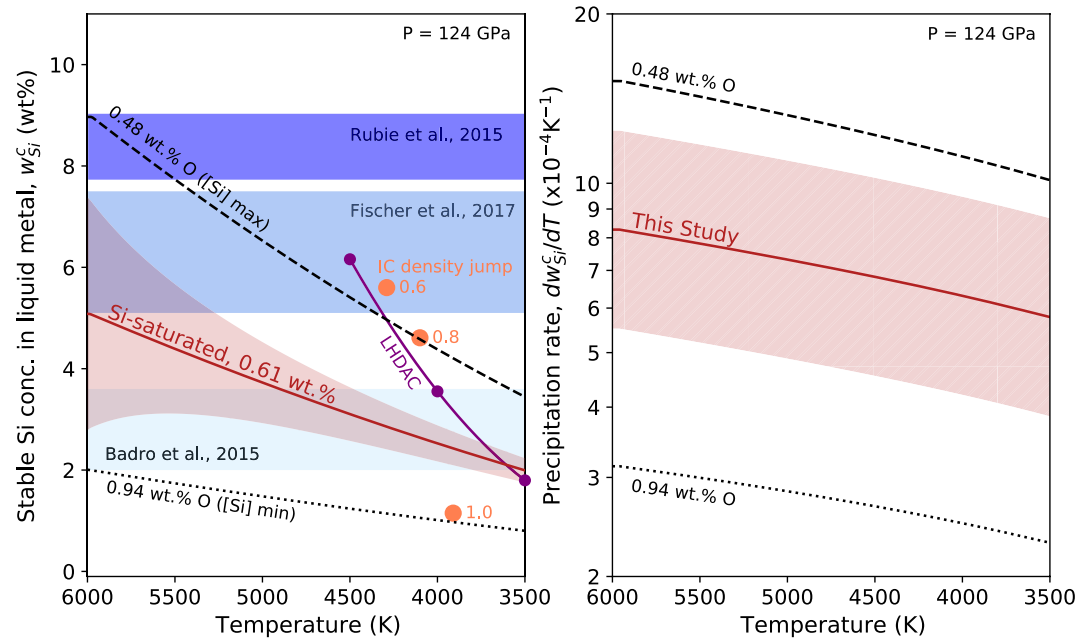
Figure 2. Left: Stable concentration of Si in liquid metal interacting with a 38.8 mol% SiO_2 silicate at 124 GPa. Our model is evaluated for liquid metal containing 0.61 wt.% O (red solid line) where Si is always at the equilibrium concentration. Red shaded envelope is the uncertainty from the fitting parameters of our model. Dotted (dashed) lines show the stable Si fraction when O concentration is set to produce initial conditions matching the minimum (maximum) Si in the liquid according to models of early core composition (Badro et al., 2015; Rubie et al., 2015). Orange circles are estimates of present-day core composition (Davies et al., 2015) (within an Fe-Si/S-O core) based on the inner core (IC) density jump of 0.6, 0.8 and 1.0 g cm^{-3}. Laser heated diamond anvil cell experiments (Hirose et al., 2017) are shown as purple circles. Horizontal shaded regions are estimated initial high (Rubie et al., 2015) (dark blue), moderate (Fischer et al., 2017) (mid blue) and low (Badro et al., 2015) (light blue) core Si content. Right: Precipitation rate from our model, hatched shaded region of 1.5x and 0.67x encompasses functional models using parameters fixed to values found from previous studies.

Si content (see Table S5 in Supporting Information S1), and with ($\alpha_{ppt}^i \neq 0$: A, B, C, D) and without ($\alpha_{ppt}^i = 0$: A^P, B^P, C^P, D^P) the convective power of precipitation included giving 8 unique scenarios. Si saturation is defined as having the thermodynamically stable fraction of Si in the core at the initial T_{cmb} and under-saturation has the stable fraction at 5500 K. For each case we vary the upper to lower mantle viscosity ratio (f_{visco}) and initial T_{cmb} (Supporting Information S1 for details) to regulate the core temperature such that the final state of our models best matches constraints of the present-day core. These constraints are: the IC radius agreeing with the present-day value of 1,221 km, a present-day mantle convective heat flow of 39 TW (Jaupart et al., 2007), a mid-mantle temperature of 2320 K, and a positive entropy from ohmic dissipation (or dynamo entropy, E_j) for all time preceding IC formation. We present cases which achieve these constraints in Figure 4. Figure 3 shows examples of the time evolution for two cases that differ by the inclusion or emission of precipitation.

The outcomes of our thermal history cases are presented in Figure 4. When Si is initially saturated (cases A, A^P and C, C^P) the low O cases require high values of f_{visco} for the IC to not grow too large by 4.5 Gyrs. In the high O cases, low temperatures are needed to freeze the IC due to enhanced melting point depression and $f_{visco} < 7$ is required in order to grow the IC to present-day size, because the mantle sets Q_{cmb} and allows rapid secular cooling. When $Q_{ppt} \neq 0$ (again for Si saturated initial conditions, cases A^P and C^P) cooling rates are lower and the IC is older than without precipitation, especially for O-poor conditions where more Si is available to precipitate (case C^P = 1,102 Myrs). For cases of initial Si undersaturation (B, B^P, D, D^P; meaning precipitation is delayed by between 370 and 1,462 Myrs when $\alpha \neq 0$), a similar core temperature is needed both with and without precipitation, however, in all compositional configurations the IC is older with precipitation power included (cf. Hirose et al., 2017). Whilst all considered cases are able to produce a geodynamo within the first 2 Gyrs, cases where $Q_{ppt} = 0$ are unable to produce a magnetic field from at least 200 Myrs prior to IC formation whilst satisfying all constraints.
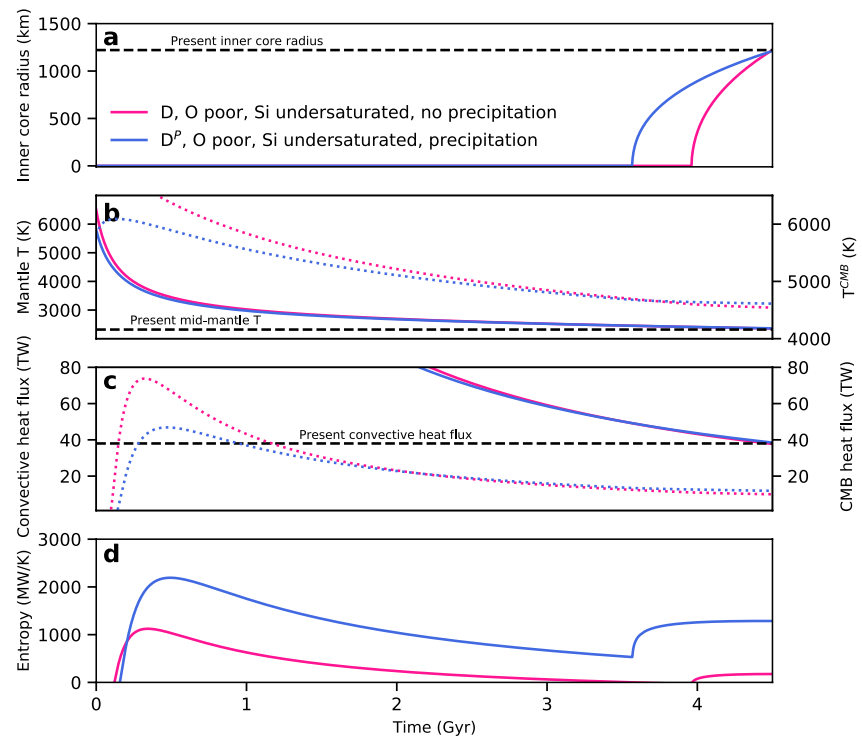
Figure 3. Thermal evolution of the Earth's core with an initial condition of 2 mol% O and Si saturation with inclusion (blue) and exclusion (pink) of power and entropy of precipitation. IC radius (a), mid-mantle potential temperature (b, left, solid lines) and T_{cmb} (b, right, dotted lines), convective mantle heat flux (c, left, solid lines) and Q_{cmb} (c, right, dotted), and E_j (d). Black dashed lines show present-day target values.

Although we include a solid mantle in our model, we do not include a BMO despite the model producing super-solidus T_{cmb} during the first 1 Gyrs. Our ab initio simulations and thermodynamic model only consider liquids, but we believe that omitting a BMO is preferable to introducing additional uncertain parameters, such as BMO viscosity and thermal conductivity, into our model. Instead, one might envisage a persistent thin melt layer at the base of the mantle, with negligible latent heat release and an equal PT of radiogenic elements (which we do not expect to be the case in reality) with the overlying mantle. We do observe sub adiabatic Q_{cmb} prior to IC formation in our models implying thermally stratified layers at the top of the liquid core. Q_{cmb} at these times (~10 TW) suggests that these layers would be less than 300 km thick (Greenwood et al., 2021) and therefore would not significantly affect the predicted cooling rate or entropy production. Whilst we hold the SiO_2 concentration of the mantle constant in our model to define the stable fraction of Si in the core, as the fraction of O in the core changes, the equilibrium concentration of FeO in the mantle will also. Using the description of FeO PT from Mittal et al. (2020), our thermal histories predict $x_{FeO}^{silicate}$ of 1.5–12 mol. %, with low O cases being <4 mol.%.

To explore the effect of uncertainty in our thermodynamic model on our result, we double and halve the calculated precipitation rate (red hashed region, Figure 2). This requires minor adjustment of initial T_{cmb} and f_{visco}, all 4 constraints can still be matched in the cases which include precipitation whilst IC ages differ by <100 Myrs and ancient core temperatures by <50 K. This shows that different combinations of interaction parameters in the thermodynamic model can produce some variance in the calculated precipitation rate, but this is not large enough to change the outcome of the thermal evolution. We also show that the uncertainty on the initial oxygen content (dashed and dotted lines, Figure 2) of the core has a far greater effect on the outcome of thermal evolution models than the uncertainty of thermodynamic modeling.

It is possible that exploring additional parameter space in our thermal history model, the geodynamo might be powered without precipitation of Si included, or other light elements can generate convective power through precipitation (Badro et al., 2018). However, we expect these cases to be rare. Davies et al. (2015) explore the uncertainty of material properties on the thermal history of the core and find that varying k, heat capacity, chemical expansivity and melting temperature individually by 10% from default values can only account for up to
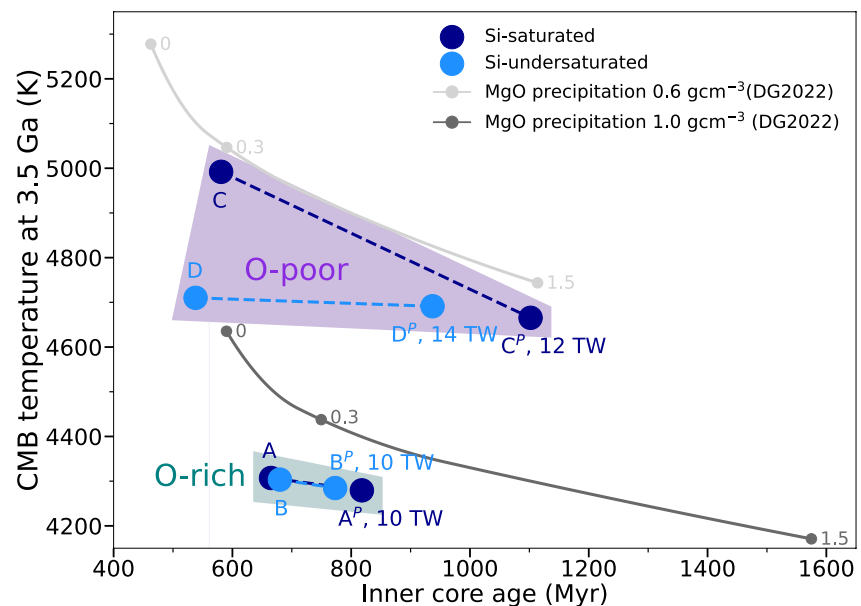
Figure 4. IC age and core temperature at 3.5 Ga for our model with and without convective power from precipitation (connected by dashed lines). Initial Si saturation (undersaturation) is shown as dark (light) blue. O rich (poor) initial conditions are captured by teal (purple) regions. Labels correspond to setup conditions in Table S5 in Supporting Information S1 and give the core mantle boundary heat flow at 3.5 Ga for models which maintain positive E_j for all time. Also shown are the results from models examining MgO precipitation (Davies & Greenwood, 2021) for precipitation rates of 0, 0.3 and 1.5×10^{-5} K^{-1}, colors denote the core properties in terms of the density jump at the IC boundary (0.6 (light gray) and 1.0 g cm^{-3} (dark gray)) which represent bounding extremes of the density jump.

200 Myrs difference to the IC age. Figure 4 shows that the uncertainty on the oxygen content of the early core can produce a difference in IC ages up to 300 Myrs. Similarly, we test the effect of varying core properties on our thermal history model. Chemical expansivity $\left(\alpha_{ppt}^{Si}\right)$, core heat capacity and k are altered by $\pm 10\%$ from reference values (from Greenwood et al., 2021) and we use an alternate Fe melting curve (Anzellini et al., 2013). Whilst this did not cause any of our $Q_{ppt} \neq 0$ models to fail, reducing α_{ppt}^{Si} moved Si undersaturated cases closer to failure and a reduced k made some cases without precipitation succeed (cf. O'Rourke et al., 2017). We do not consider lower k values since it is well known that core-mantle evolution models can satisfy the four constraints in this scenario. When increased to 100 W m^{-1} K^{-1} we find that cases where Si is initially undersaturated, and therefore precipitation is delayed, can fail. This demonstrates the finite power available from Si precipitation, especially if high O concentration limits the Si dissolved into the early core. Other parameterisations of mantle evolution might offer models with positive E_j, but this has so far not proved correct in the work of O'Rourke et al. (2017) (who used the parameterization of Korenaga (2006) or Nakagawa and Tackley (2014) (who conducted 3D self-consistent simulations of mantle convection).

5. Conclusions

We find that precipitation of Si allows the early core to cool more slowly than it would otherwise and can supply power to the geodynamo throughout Earth's history. High O concentration in the core can reduce ancient core temperatures by 400–700 K but relies predominantly on secular cooling to power the ancient geodynamo, meaning failure for higher k than considered here. More plausible low O cases result in higher ancient CMB temperatures (4700–5000 K) due to lesser melting point depression. The rheological transition of the magma ocean should occur between 40% and 60% melt fraction (Abe, 1997; Solomatov, 2015) at ~4500 K, rather than at the intersection of the liquidus or solidus, which would correspond to the occurrence of complete crystallisation and first partial melt, respectively. Our thermal histories for low O content in particular suggest a long lived BMO. A high k scenario where the ancient geodynamo is powered by Si precipitation places constraint on accretionary models of core composition. We show that an initial core composition of 4.3 wt.% Si and 1.1 wt.% O is both thermodynamically stable and able to produce sufficient power for the ancient geodynamo to be sustained in a

high *k* core, this limits compatible accretion models to those which predict intermediate initial core Si content and low O content.

Data Availability Statement

Details of ab initio calculations and thermodynamic modelling are available in the Supporting Information S1 and the Zenodo deposit. Our experimental data set as well as the list of included studies can be found at https://zenodo.org/record/7274785#.Y2pk8-zP1qs. Thermal evolution models were provided by Sam Greenwood and is freely available at https://github.com/sam-greenwood/thermal_history.git.

References

Abe, Y. (1997). Thermal and chemical evolution of the terrestrial magma ocean. *Physics of the Earth and Planetary Interiors*, *100*(1–4), 27–39. https://doi.org/10.1016/s0031-9201(96)03229-3

Alfè, D., Gillan, M., & Price, G. D. (2002). Composition and temperature of the Earth's core constrained by combining ab initio calculations and seismic data. *Earth and Planetary Science Letters*, *195*(1–2), 91–98. https://doi.org/10.1016/s0012-821x(01)00568-4

Anzellini, S., Dewaele, A., Mezouar, M., Loubeyre, P., & Morard, G. (2013). Melting of iron at Earth's inner core boundary based on fast X-ray diffraction. *Science*, *340*(6131), 464–466. https://doi.org/10.1126/science.1233514

Badro, J., Aubert, J., Hirose, K., Nomura, R., Blanchard, I., Borensztajn, S., & Siebert, J. (2018). Magnesium partitioning between Earth's mantle and core and its potential to drive an early exsolution geodynamo. *Geophysical Research Letters*, *45*(24), 13–240. https://doi.org/10.1029/2018gl080405

Badro, J., Brodholt, J. P., Piet, H., Siebert, J., & Ryerson, F. J. (2015). Core formation and core composition from coupled geochemical and geophysical constraints. *Proceedings of the National Academy of Sciences*, *112*(40), 12310–12314. https://doi.org/10.1073/pnas.1505672112

Badro, J., Siebert, J., & Nimmo, F. (2016). An early geodynamo driven by exsolution of mantle components from Earth's core. *Nature*, *536*(7616), 326–328. https://doi.org/10.1038/nature18594

Braginsky, S. (1963). Structure of the f layer and reasons for convection in the Earth's core. In *Proceedings of the USSR Academy of Sciences* (Vol. 149, pp. 8–10).

Buffett, B. A., Huppert, H. E., Lister, J. R., & Woods, A. W. (1996). On the thermal evolution of the Earth's core. *Journal of Geophysical Research*, *101*(B4), 7989–8006. https://doi.org/10.1029/95jb03539

Chidester, B. A., Rahman, Z., Righter, K., & Campbell, A. J. (2017). Metal–silicate partitioning of u: Implications for the heat budget of the core and evidence for reduced u in the mantle. *Geochimica et Cosmochimica Acta*, *199*, 1–12. https://doi.org/10.1016/j.gca.2016.11.035

Davies, C. (2015). Cooling history of Earth's core with high thermal conductivity. *Physics of the Earth and Planetary Interiors*, *247*, 65–79. https://doi.org/10.1016/j.pepi.2015.03.007

Davies, C., & Greenwood, S. (2021). Dynamics in Earth's core arising from thermo-chemical interactions with the mantle. In *Core Mantle Coevolution - A multidisciplinary approach*. Wiley. (in Press).

Davies, C., Pozzo, M., Gubbins, D., & Alfè, D. (2015). Constraints from material properties on the dynamics and evolution of Earth's core. *Nature Geoscience*, *8*(9), 678–685. https://doi.org/10.1038/ngeo2492

de Koker, N., Steinle-Neumann, G., & Vlček, V. (2012). Electrical resistivity and thermal conductivity of liquid Fe alloys at high P and T, and heat flux in Earth's core. *Proceedings of the National Academy of Sciences*, *109*(11), 4070–4073. https://doi.org/10.1073/pnas.1111841109

Driscoll, P., & Bercovici, D. (2014). On the thermal and magnetic histories of Earth and Venus: Influences of melting, radioactivity, and conductivity. *Physics of the Earth and Planetary Interiors*, *236*, 36–51. https://doi.org/10.1016/j.pepi.2014.08.004

Du, Z., Boujibar, A., Driscoll, P., & Fei, Y. (2019). Experimental constraints on an MgO exsolution-driven geodynamo. *Geophysical Research Letters*, *46*(13), 7379–7385. https://doi.org/10.1029/2019gl083017

Du, Z., Jackson, C., Bennett, N., Driscoll, P., Deng, J., Lee, K. K., et al. (2017). Insufficient energy from MgO exsolution to power early geodynamo. *Geophysical Research Letters*, *44*(22), 11–376. https://doi.org/10.1002/2017gl075283

Fischer, R. A., Campbell, A. J., & Ciesla, F. J. (2017). Sensitivities of Earth's core and mantle compositions to accretion and differentiation processes. *Earth and Planetary Science Letters*, *458*, 252–262. https://doi.org/10.1016/j.epsl.2016.10.025

Fischer, R. A., Nakajima, Y., Campbell, A. J., Frost, D. J., Harries, D., Langenhorst, F., et al. (2015). High pressure metal–silicate partitioning of Ni, Co, V, Cr, Si, and O. *Geochimica et Cosmochimica Acta*, *167*, 177–194. https://doi.org/10.1016/j.gca.2015.06.026

Gomi, H., Ohta, K., Hirose, K., Labrosse, S., Caracas, R., Verstraete, M. J., & Hernlund, J. W. (2013). The high conductivity of iron and thermal evolution of the Earth's core. *Physics of the Earth and Planetary Interiors*, *224*, 88–103. https://doi.org/10.1016/j.pepi.2013.07.010

Greenwood, S., Davies, C. J., & Mound, J. E. (2021). On the evolution of thermally stratified layers at the top of Earth's core. *Physics of the Earth and Planetary Interiors*, *318*, 106763. https://doi.org/10.1016/j.pepi.2021.106763

Gubbins, D., Alfè, D., Masters, G., Price, G. D., & Gillan, M. (2004). Gross thermodynamics of two-component core convection. *Geophysical Journal International*, *157*(3), 1407–1414. https://doi.org/10.1111/j.1365-246x.2004.02219.x

Helffrich, G., Hirose, K., & Nomura, R. (2020). Thermodynamical modeling of liquid Fe-Si-Mg-O: Molten magnesium silicate release from the core. *Geophysical Research Letters*, *47*(21), e2020GL089218. https://doi.org/10.1029/2020gl089218

Hirose, K., Morard, G., Sinmyo, R., Umemoto, K., Hernlund, J., Helffrich, G., & Labrosse, S. (2017). Crystallization of silicon dioxide and compositional evolution of the Earth's core. *Nature*, *543*(7643), 99–102. https://doi.org/10.1038/nature21367

Hohenberg, P., & Kohn, W. (1964). Inhomogeneous electron gas. *Physical Review*, *136*(3B), B864–B871. https://doi.org/10.1103/physrev.136.b864

Hsieh, W.-P., Goncharov, A. F., Labrosse, S., Holtgrewe, N., Lobanov, S. S., Chuvashova, I., et al. (2020). Low thermal conductivity of iron-silicon alloys at Earth's core conditions with implications for the geodynamo. *Nature Communications*, *11*(1), 1–7. https://doi.org/10.1038/s41467-020-17106-7

Jaupart, C., Labrosse, S., Lucazeau, F., & Mareschal, J. (2007). 7.06-temperatures, heat and energy in the mantle of the Earth. *Treatise on geophysics*, *7*, 223–270.

Kohn, W., & Sham, L. J. (1965). Self-consistent equations including exchange and correlation effects. *Physical Review*, *140*(4A), A1133–A1138. https://doi.org/10.1103/physrev.140.a1133

Korenaga, J. (2006). Archean geodynamics and the thermal evolution of Earth. *Geophysical Monograph-American Geophysical Union*, *164*, 7.

Labrosse, S. (2015). Thermal evolution of the core with a high thermal conductivity. *Physics of the Earth and Planetary Interiors*, *247*, 36–55. https://doi.org/10.1016/j.pepi.2015.02.002

Li, Y., Vočadlo, L., Alfè, D., & Brodholt, J. (2019). Carbon partitioning between the Earth's inner and outer core. *Journal of Geophysical Research: Solid Earth*, *124*(12), 12812–12824. https://doi.org/10.1029/2019jb018789

Liu, W., Zhang, Y., Yin, Q.-Z., Zhao, Y., & Zhang, Z. (2020). Magnesium partitioning between silicate melt and liquid iron using first-principles molecular dynamics: Implications for the early thermal history of the Earth's core. *Earth and Planetary Science Letters*, *531*, 115934. https://doi.org/10.1016/j.epsl.2019.115934

Ma, Z. (2001). Thermodynamic description for concentrated metallic solutions using interaction parameters. *Metallurgical and Materials Transactions B*, *32*(1), 87–103. https://doi.org/10.1007/s11663-001-0011-0

Mittal, T., Knezek, N., Arveson, S. M., McGuire, C. P., Williams, C. D., Jones, T. D., & Li, J. (2020). Precipitation of multiple light elements to power Earth's early dynamo. *Earth and Planetary Science Letters*, *532*, 116030. https://doi.org/10.1016/j.epsl.2019.116030

Nakagawa, T., & Tackley, P. J. (2013). Implications of high core thermal conductivity on Earth's coupled mantle and core evolution. *Geophysical Research Letters*, *40*(11), 2652–2656. https://doi.org/10.1002/grl.50574

Nakagawa, T., & Tackley, P. J. (2014). Influence of combined primordial layering and recycled morb on the coupled thermal evolution of Earth's mantle and core. *Geochemistry, Geophysics, Geosystems*, *15*(3), 619–633. https://doi.org/10.1002/2013gc005128

Nimmo, F. (2015). Energetics of the core. In G. Schubert (Ed.), *Treatise on geophysics* (2nd ed., Vol. 8, pp. 27–55). Elsevier.

O'Rourke, J. G., Korenaga, J., & Stevenson, D. J. (2017). Thermal evolution of Earth with magnesium precipitation in the core. *Earth and Planetary Science Letters*, *458*, 263–272. https://doi.org/10.1016/j.epsl.2016.10.057

O'Rourke, J. G., & Stevenson, D. J. (2016). Powering Earth's dynamo with magnesium precipitation from the core. *Nature*, *529*(7586), 387–389. https://doi.org/10.1038/nature16495

Pozzo, M., Davies, C., Gubbins, D., & Alfè, D. (2012). Thermal and electrical conductivity of iron at Earth's core conditions. *Nature*, *485*(7398), 355–358. https://doi.org/10.1038/nature11031

Pozzo, M., Davies, C., Gubbins, D., & Alfè, D. (2013). Transport properties for liquid silicon-oxygen-iron mixtures at Earth's core conditions. *Physical Review B*, *87*(1), 014110. https://doi.org/10.1103/physrevb.87.014110

Pozzo, M., Davies, C., Gubbins, D., & Alfè, D. (2019). FeO content of Earth's liquid core. *Physical Review X*, *9*(4), 041018. https://doi.org/10.1103/physrevx.9.041018

Pozzo, M., Davies, C. J., & Alfè, D. (2022). Towards reconciling experimental and computational determinations of Earth's core thermal conductivity. *Earth and Planetary Science Letters*, *584*, 117466. https://doi.org/10.1016/j.epsl.2022.117466

Rubie, D. C., Jacobson, S. A., Morbidelli, A., O'Brien, D. P., Young, E. D., de Vries, J., et al. (2015). Accretion and differentiation of the terrestrial planets with implications for the compositions of early-formed solar system bodies and accretion of water. *Icarus*, *248*, 89–108. https://doi.org/10.1016/j.icarus.2014.10.015

Solomatov, V. (2015). Magma oceans and primordial mantle differentiation. In G. Schubert (Ed.), *Treatise on geophysics* (Vol. 10, pp. 81–104). Elsevier.

Takafuji, N., Hirose, K., Mitome, M., & Bando, Y. (2005). Solubilities of O and Si in liquid iron in equilibrium with (Mg, Fe) Sio3 perovskite and the light elements in the core. *Geophysical Research Letters*, *32*(6), L06313. https://doi.org/10.1029/2005gl022773

Tarduno, J. A., Cottrell, R. D., Watkeys, M. K., Hofmann, A., Doubrovine, P. V., Mamajek, E. E., et al. (2010). Geodynamo, solar wind, and magnetopause 3.4 to 3.45 billion years ago. *Science*, *327*(5970), 1238–1240. https://doi.org/10.1126/science.1183445

Zhang, Z., Csányi, G., Alfè, D., Zhang, Y., Li, J., & Liu, J. (2022). Free energies of Fe-O-Si ternary liquids at high temperatures and pressures: Implications for the evolution of the Earth's core composition. *Geophysical Research Letters*, *49*(4), e2021GL096749. https://doi.org/10.1029/2021gl096749